CrossMark

Ni(II) removal from aqueous solution by biosorption and flocculation using microbial flocculant GA1

Yan Zhou[1,2] · **Zhao-hui Yang**[1,2] · **Jing Huang**[1,2] ·
Rui Xu[1,2] · **Pei-pei Song**[1,2] · **Yi-jie Zhang**[1,2] ·
Juan Li[1,2] · **Manosane Aloun**[1,2]

Abstract Generally, most biomaterials present high biosorption capacity for heavy-metal ions. In this study, alkaline reagents and microbial flocculant GA1 (MBFGA1) were combined to remove Ni(II) from aqueous solution. Response surface methodology was employed to optimize the flocculation and biosorption conditions with the Ni(II) removal rate as the response, as well as to analyze the biosorption capacity. At initial Ni(II) concentration of 100 mg L^{-1}, the optimal conditions were predicted to be 1.3×10^{-2}% (w/w) CaO, 6.59×10^{-3}% (w/w) MBFGA1, and stirring time of 61.97 min, at which the Ni(II) removal rate and biosorption capacity of MBFGA1 could reach 99.35% and 225.16 mg g^{-1}, respectively. The biosorption behavior, Fourier-transform infrared spectra, and environmental scanning electron microscopy analysis demonstrated that adsorption bridging with precipitation enmeshment was the most likely mechanism. Analysis of the mechanism and procedure indicated that synergistic flocculation and biosorption by MBFGA1 resulted in the significant Ni(II) removal.

Keywords Microbial flocculant · Biosorption · Flocculation · Ni(II) · Collaboration

✉ Zhao-hui Yang
    yzh@hnu.edu.cn

1   College of Environmental Science and Engineering, Hunan University,
    Changsha 410082, People's Republic of China

2   Key Laboratory of Environmental Biology and Pollution Control (Hunan University), Ministry
    of Education, Changsha 410082, People's Republic of China

Introduction

Ni(II) is a toxic heavy metal present in wastewater from industries such as electroplating, battery manufacture, mining, metal finishing and forging, paint formulation, porcelain enameling, and steam–electric power plants [1, 2]. Above permissible exposure levels, Ni(II) has potential to produce a variety of pathological effects on humans, including contact dermatitis, lung fibrosis, and cardiovascular and kidney diseases [3], and can even cause lung, nose, and bone cancer [4, 5]. Therefore, effective treatment of industrial effluents to remove Ni(II) is of primary importance to human life and health. Removal of Ni(II) ions can be accomplished by a variety of methods, such as chemical precipitation, adsorption, ion exchange, electrochemical methods, etc. Although such methods achieve high removal rates and offer various other advantages, they also suffer from many limitations. Many previous studies have reported that adsorbents have only low adsorption capacity [6–9]; in other words, it is necessary to enhance the efficiency of adsorbents. Ion exchange offers high treatment capacity, but the resins applied need to be rejuvenated regularly [10, 11]. Electrochemical methods consume large amounts of electricity [12–14]. It is well known that chemical precipitation is the most widely used method for removal of Ni(II) ions, but the pH must be raised to 9–10 and subsequent processing is required in most cases [15]. Meanwhile, chemical precipitation is often combined with other chemical reagents to remove metal ions, e.g., chemical flocculants such as polymeric aluminum chloride (PAC) and polyacrylamide (PAM). Nonetheless, chemical flocculants may cause some health and environmental problems; For instance, when PAC is used, residual aluminum may result in high incidence of Alzheimer's disease, while PAM is neurotoxic, carcinogenic, and nonbiodegradable [16–20]. So, a high-efficiency and more environmentally friendly material is essential. In this study, a particular microbial flocculant (MBF) was employed to remove Ni(II) ions via chemical precipitation.

Because of their high efficiency, low toxicity, and biodegradability, MBFs are being used for removal of heavy metals by increasing numbers of researchers. In many studies utilizing MBFs to remove heavy metals from wastewater [21–23], the conventional biosorption method is used, followed by centrifugation and filtration to separate the heavy metals. In such approaches, the biosorption has a great effect on the removal of heavy metals, but the flocculation performance of MBFs is not considered. Therefore, the full benefits of MBFs are not achieved. In addition, MBFs mainly occur in dissolved form in water, so the large residual amount in the supernatant after treatment could still adsorb a certain amount of heavy metals, and the complex generated is difficult to separate. Therefore, a carrier is needed to complete the final solid–liquid separation process after biosorption; this carrier could combine flocculation with biosorption of MBFs to make full use of the advantages of MBFs.

It is generally known that neutralization precipitation is a method with good adaptability and economical processing, and that heavy-metal ions in wastewater can precipitate as insoluble hydroxides on addition of alkaline reagents [24]. Some studies have shown that the combination of neutralization precipitation and MBFs

could more effectively improve the efficiency of heavy-metal removal and facilitate subsequent sludge treatment [25, 26]. Nevertheless, such studies usually focus on the reinforcing effect of flocculation on removal via heavy-metal precipitation, premised on the condition that the dissolved heavy-metal ions can fully form hydroxide precipitates, which can be indirectly achieved by adjusting the pH when MBFs are used for removal of heavy-metal ions. Therefore, MBFs seem to represent a good type of carrier for use in heavy-metal hydroxide precipitation after biosorption for solid–liquid separation. We use the term "incomplete neutralization precipitation" to indicate the case where only part of the dissolved heavy-metal ions can form hydroxide precipitates. Consequently, in incomplete neutralization precipitation, part of the formed hydroxide precipitate can be used as a carrier, which is conducive to the combination of flocculation and biosorption; not only might the carriers act as cores for the flocculation process, but they may also provide attachment points for MBFs after the biosorption process.

It is believed that flocculation is the basis of biosorption, which itself supplements and promotes flocculation. Based on this concept, use of incomplete neutralization precipitation to develop a suitable flocculation and biosorption system becomes an interesting approach. On the one hand, addition of MBFs can promote aggregation and sedimentation of heavy-metal hydroxides, while on the other hand, active groups of MBFs can adsorb dissolved heavy-metal ions and then coprecipitate with heavy-metal hydroxides present in the wastewater. Moreover, due to the condition of incomplete neutralization precipitation, both the pH and the generation of precipitates in the system would be relatively low afterwards, potentially facilitating subsequent processing in practical applications. Therefore, it is significant to investigate the collaboration between flocculation and biosorption when using MBFs in treatment processes for wastewater containing heavy metals under the condition of incomplete neutralization precipitation.

In this study, two kinds of alkaline reagent (CaO, NaOH) and MBFGA1 were combined to remove Ni(II) from aqueous solution, and the differences between their experimental results analyzed under the condition of incomplete neutralization precipitation. Response surface methodology (RSM) was employed to optimize the flocculation and biosorption conditions using the Ni(II) removal rate as the response. Meanwhile, the biosorption behavior of MBFGA1 was investigated. Moreover, the mechanism and procedure of the collaboration between flocculation and biosorption are explored based on experimental characterization.

Materials and methods

Reagents

HNO_3 stock solution was prepared at volume fraction of 0.5%. $Ni(NO_3)_2 \cdot 6H_2O$ was dissolved by a certain amount of 0.5% HNO_3, and Ni(II) stock solution was prepared at concentration of 1 g L^{-1}. In this study, CaO and NaOH were alkaline reagents used to adjust the pH and to promote flocculation and biosorption. NaOH

was used for comparison. NaOH and HCl were prepared at concentration of 0.2 mol L^{-1}. All the above-mentioned reagents were analytically pure.

Preparation of MBFGA1

MBFGA1 is a microbial flocculant harvested from fermentation liquid of *Paenibacillus polymyxa* GA1 [17], being an extracellular polymeric substance (EPS) with variable molecular mass and structural properties, including many polysaccharides, a few proteins, and nucleic acids [27].

Bacterial strain and culture conditions

GA1, flocculant-producing strain CCTCC M206017, identified as *Paenibacillus polymyxa* according to its 16S ribosomal DNA (rDNA) sequence and biochemical and physiological characteristics, was screened from soil collected at Yuelu Mountain, Changsha, China [17]. Seed medium and fermentation medium were prepared as described previously [28]. After cultivation, fermentation liquid with 16.55 g L^{-1} effective components was stored at 4 °C before use.

Extraction and purification

Fermentation liquid was centrifuged at 6000 rpm for 30 min, then the supernatant was poured into two volumes of cold acetone (4 °C) to precipitate microbial flocculant. The mixture was placed in a refrigerator of 4 °C for 24 h to stabilize the precipitate; subsequently, the precipitate was collected by centrifugation at 4000 rpm for 30 min. The precipitate was dissolved by a moderate amount of distilled water, then placed in a refrigerator at −24 °C for 24 h. Next, crude microbial flocculant was obtained by vacuum freeze-drying.

Crude microbial flocculant was ground and dissolved in distilled water. Subsequently, the samples were poured into two volumes of Sevage reagents (chloroform:N-butyl alcohol = 5:1) and subjected to sufficient vibration for 60 min. The supernatant was collected after 5 min of standing in a separating funnel. After five such purification steps of deproteinization, the samples were extracted again with cold acetone (4 °C), then the samples were placed in a rotary evaporator (R206, SENCO, China) at 40 °C for 1 h to remove acetone and residual organic solvent. Next, the products were ground and dissolved in distilled water, and the samples were dialyzed at 4 °C for 24 h in deionized water. Subsequently, they were placed in a rotary evaporator again to concentration. Finally, fine microbial flocculant was obtained by vacuum freeze-drying and used in characterization experiments [29].

Flocculation and biosorption tests

A standard jar tester was used for flocculation and biosorption tests using aqueous Ni(II) solution dosed with MBFGA1. A beaker with capacity of 800 mL was injected with 500 mL aqueous Ni(II) solution then fixed on a floc tester (ET-720, Lovibond, Germany). The pH of the mixture was adjusted using alkaline reagents

(CaO and NaOH), and quantitative NaOH was injected by peristaltic pump (BT100-1L, LongerPump, China) at flow rate of 2000 μL min^{-1}; to reduce errors, all the NaOH solution was injected with different volumes of distilled water to reach 10 mL. After each addition, the reaction was performed with rapid mixing at 150 rpm for 60 s, followed by slow mixing at 50 rpm for designated duration. After 5 min of standing, the supernatant for measurement was collected by pipette. The variation of the zeta potential during the process of pH adjustment using the alkaline reagents was measured by Zetasizer (Nano-ZS90, Malvern, UK). Flocculation mainly occurred during the rapid mixing stage, and biosorption mainly during the slow mixing stage [17, 30]. The effects of the MBFGA1 dose, NaOH dose, and mixing time on the Ni(II) removal rate and biosorption capacity of MBFGA1 were investigated. The Ni(II) concentration was determined by inductively coupled plasma-atomic emission spectrometry (PS-6, Baird, USA) after filtering through a 0.45-μm membrane. The Ni removal rate and biosorption capacity of MBFGA1 were calculated as follows:

$$\text{Removal rate } (\%) = (C_0 - C_a)/C_0 \times 100\%, \tag{1}$$

$$\text{Biosorption capacity } \left(\text{mg g}^{-1}\right) = (C_b - C_a)V/w_{GA1}, \tag{2}$$

where C_0 and C_a (mg L^{-1}) are the Ni(II) concentration initially and after flocculation and biosorption, respectively, C_b (mg L^{-1}) is the Ni(II) concentration when adding only CaO or NaOH during flocculation and biosorption, V (L) is the volume of Ni(II) solution, and w_{GA1} (g) is the weight of MBFGA1.

Studies on the biosorption isotherm were conducted at different temperatures (298, 303, and 313 K) by adding $1.3 \times 10^{-2}\%$ (w/w) CaO and $6.62 \times 10^{-3}\%$ (w/w) MBFGA1 into 500 mL Ni(II) solution at different initial concentrations (80, 85, 90, 95, 100, 120, and 150 mg L^{-1}) before stirring for 30 min. The experimental temperature was controlled by bolt electric heating rods. The biosorption kinetics was investigated by adding $1.3 \times 10^{-2}\%$ (w/w) CaO and $6.62 \times 10^{-3}\%$ (w/w) MBFGA1 to 500 mL of 100 mg L^{-1} Ni(II) solution, then stirring at 313 K for designated durations (0, 30, 60, 90, 120, 150, 300, and 600 min).

RSM experimental design

The central composite design (CCD), a standard RSM, was selected for optimization of three factors affecting the flocculation and biosorption: dose of alkaline reagent (CaO) (x_1), MBFGA1 (x_2), and stirring time (x_3), each at five levels. The response variable (y), i.e., the removal rate after flocculation and biosorption, was fit using a second-order model in the form of the following quadratic polynomial equation:

$$y = \beta_0 + \sum_{i=1}^{m} \beta_i x_i + \sum_{i<j}^{m} \beta_{ij} x_i x_j + \sum_{i=1}^{m} \beta_{ii} x_i^2, \tag{3}$$

where y is the response variable to be modeled, x_i and x_j are the independent variables that determine y, and β_0, β_i, and β_{ii} are the offset term, linear coefficient,

and quadratic coefficient for factor i, respectively. β_{ij} is the term capturing the interaction between x_i and x_j.

Fourier-transform infrared (FT-IR) spectra and environmental scanning electron microscopy (ESEM) analysis

Samples of original and Ni(II)-loaded MBFGA1 were obtained after vacuum freeze-drying. To study the interactions between the Ni(II) ions and MBFGA1, Fourier-transform infrared spectrometry (Tensor 27, Bruker, Germany) was applied to analyze the functional groups present in the samples.

Besides the above-mentioned samples, flocs obtained by adding only alkaline reagent (CaO) and MBFGA1 to flocculate and adsorb Ni(II) under the optimal experimental conditions were collected and subjected to vacuum freeze-drying. The surface morphology of these samples was analyzed by environmental scanning electron microscopy (Quanta 200 FEG, FEI, USA) in low-vacuum mode at accelerating potential of 20 kV. In addition, microanalysis of the collected samples was carried out by energy-dispersive spectrometry (EDS) equipped on the Quanta 200.

Results and discussion

Effect of alkaline reagents (NaOH and CaO) on zeta potential and pH

To achieve neutralization and sedimentation of heavy metals, quantitative alkaline reagents (NaOH and CaO) were added into 500 mL simulated Ni(II)-containing wastewater (100 mg L^{-1}) to study the variation of the zeta potential and pH. The initial pH and zeta potential of the simulated wastewater were 3.21 and −10.01 mV, respectively. Figure 1 shows the variation of the zeta potential of the generated hydroxide suspension system, exhibiting the same rising, plateau, and declining periods after addition of the different alkaline reagents. As seen from Fig. 1a, after addition of quantitative NaOH, the pH of the Ni(II) wastewater increased from 3.52 to 9.83 while the zeta potential increased from −5.79 to 30.5 mV then dropped to 11.8 mV. The period of zeta potential increase was relatively drastic, indicating that the insoluble metal salt quickly precipitated with addition of the alkaline reagents. The zeta potential plateau period was comparatively stable; in this case, Ni(II) continually consumed newly produced hydroxyl ions in solution and separated out more insoluble metal salt quickly from the wastewater, as shown by the slow increase of pH. The period of zeta potential decline was relatively drastic, which may suggest that most of the Ni(II) had been converted to hydroxides. Therefore, the stability of the whole colloid system began to decrease and then the hydroxides would agglomerate, while the pH of the wastewater changed drastically. In Fig. 1b, the same pattern of changes can be seen after adding quantitative CaO: the pH of the Ni(II)-containing wastewater increased from 7.84 to 11.23 while the zeta potential increased from 26.5 to 39.6 mV then dropped to 31.9 mV. According to this
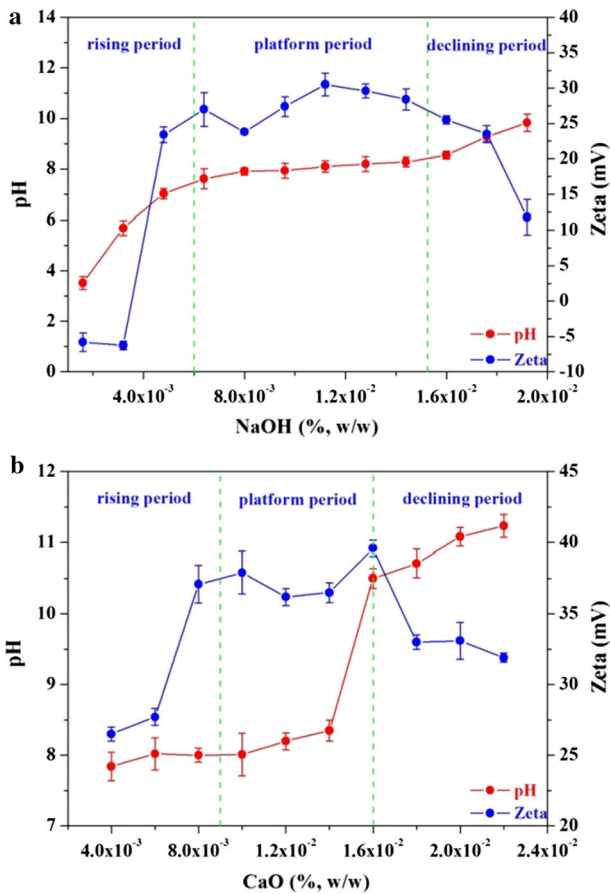
Fig. 1 Variation of zeta potential and pH of Ni(II)-containing wastewater after addition of alkaline reagents (NaOH and CaO)

analysis, if MBFGA1 were added during the period of rising zeta potential, there would be insufficient carrier for the hydroxides and the removal rate would be very low, whereas if MBFGA1 were added during the period of declining zeta potential, the high pH would convert most of the Ni(II) to hydroxides and the MBFGA1 would not exhibit its full biosorption performance. Therefore, to lower the pH and achieve the full flocculation and biosorption performance of MBFGA1, the plateau period was selected for subsequent experiments, in other words, incomplete neutralization precipitation.

Effect of MBFGA1 dose on flocculation and biosorption

According to the experimental results presented above, three points (left, middle, and right) in the zeta potential plateau were chosen for the experiments described in this section. The effect of the MBFGA1 dose on the flocculation and biosorption

was investigated by adding $6.0 \times 10^{-3}\%$, $1.12 \times 10^{-2}\%$, or $1.52 \times 10^{-2}\%$ (w/w) NaOH or $9.0 \times 10^{-3}\%$, $1.2 \times 10^{-2}\%$, or $1.6 \times 10^{-2}\%$ (w/w) CaO with different doses of MBFGA1 into 500 mL of 100 mg L^{-1} Ni(II) solution with stirring time of 30 min. Firstly, alkaline reagents were added with 5 min of slow stirring, then MBFGA1 was added before 1 min of rapid stirring. Figure 2a shows that the Ni(II) removal rate changed little when adding different doses of NaOH, only increasing by approximately 3% at most after addition of MBFGA1. However, Fig. 2c shows that the Ni(II) removal rate first increased then declined when adding $9.0 \times 10^{-3}\%$ (w/w) CaO and $1.2 \times 10^{-2}\%$ (w/w) CaO, increasing by approximately 12% at most after adding MBFGA1. The removal rate remained basically unchanged when adding $1.6 \times 10^{-2}\%$ (w/w) CaO, because the excess dose of CaO and the sufficiently high pH level resulted in nearly complete neutralization precipitation of Ni(II). Moreover, there is an obvious difference between Fig. 2b and d: the maximum biosorption capacity of MBFGA1 could reach about 161.63 mg g^{-1} after adding $6.62 \times 10^{-3}\%$ (w/w) MBFGA1 and $1.2 \times 10^{-2}\%$ (w/w) CaO; nevertheless, the maximum biosorption capacity of MBFGA1 only reached about 84.59 mg g^{-1} after adding $3.31 \times 10^{-3}\%$ (w/w) MBFGA1 and $1.12 \times 10^{-2}\%$ (w/w) NaOH. These results suggest that CaO is a more appropriate alkaline reagent than NaOH. The reason may be that CaO would generate Ca^{2+} and $Ca(OH)_2$ when added to aqueous solution. Ca^{2+} plays an important role in promoting flocculation of MBFGA1 [31, 32]. Moreover, as mentioned above, $Ca(OH)_2$ as a carrier could
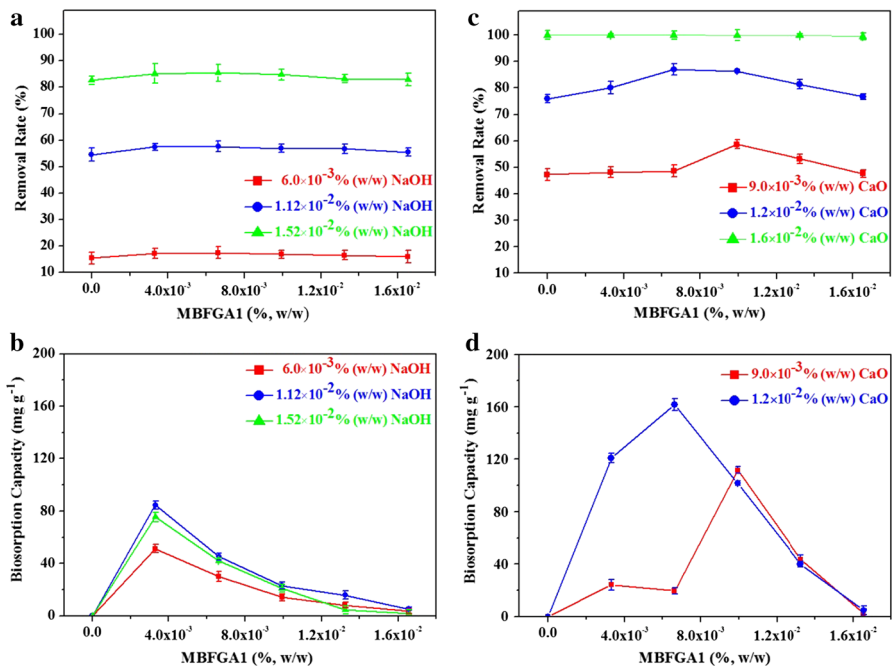
Fig. 2 Effect of MBFGA1 dose on flocculation and biosorption when adding different alkaline reagents: a, b NaOH, c, d CaO

provide cores for the flocculation process as well as attachment points for MBFGA1 after biosorption of Ni(II). Therefore, CaO was chosen as the alkaline reagent for subsequent optimization experiments.

Effect of stirring time on flocculation and biosorption

The effect of the stirring time on the flocculation and biosorption by MBFGA1 was studied simultaneously by setting different stirring times and adding $1.2 \times 10^{-2}\%$ (w/w) CaO and $6.62 \times 10^{-3}\%$ (w/w) MBFGA1 or $1.52 \times 10^{-2}\%$ (w/w) NaOH and $6.62 \times 10^{-3}\%$ (w/w) MBFGA1 into 500 mL of 100 mg L^{-1} Ni(II) solution. The results of these experiments are shown in Fig. 3. Figure 3 shows that the removal rate and biosorption capacity exhibited the same pattern of changes when adding CaO, increasing to a maximum value for stirring time of 90 min and then remaining comparatively stable. In that case, the removal rate increased from 78.37 to 94.80% while the biosorption capacity increased from 24.90 to 190.32 mg g^{-1}. These results suggest that the biosorption capacity of MBFGA1 would rise with increasing stirring time and reach a saturation value, then remain stable thereafter. However, Fig. 3 shows that the variations of the removal rate and biosorption capacity were very small when adding NaOH and MBFGA1 into Ni(II) solution. Consequently, these experimental data also prove that CaO was a more appropriate alkaline reagent in this research.

Experimental results of RSM

According to the experimental results described above, the actual design obtained using Design-Expert 8.0.6 statistical software (Stat-Ease Inc., USA) is presented in Table 1. The results for 20 groups of experiments performed according to this experimental plan are presented in Table 2. An empirical relationship between the removal rate (y) and the three factors ($x_1 - x_3$) was obtained according to the following quadratic polynomial, where the variables take coded values:
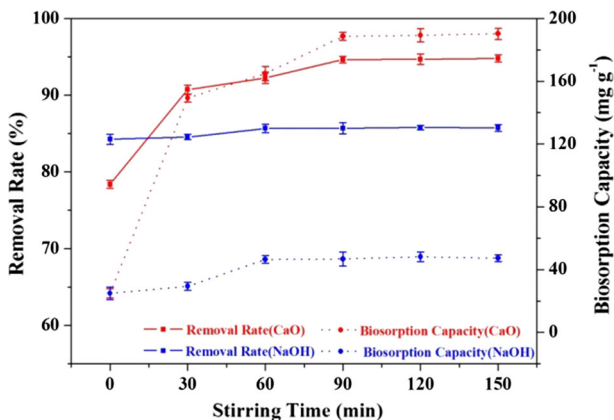
Fig. 3 Effect of stirring time on flocculation and biosorption using CaO and NaOH

Table 1 Coded levels for the three variables in the CCD

Factor	Code	Coded level				
		−1.682	−1	0	1	1.682
CaO (%, w/w)	x_1	6.0×10^{-3}	8.0×10^{-3}	1.2×10^{-2}	1.4×10^{-2}	1.6×10^{-2}
MBFGA1 (%, w/w)	x_2	0	3.34×10^{-3}	8.28×10^{-3}	1.32×10^{-2}	1.66×10^{-2}
Stirring time (min)	x_3	0	24.32	60.00	95.68	120.00

Table 2 Coded values for experimental design and results for removal rate

Run	Coded value			Removal rate (%)
	CaO (x_1)	MBFGA1 (x_2)	Stirring time (x_3)	
1	0	0	0	90.73
2	0	0	1.682	88.98
3	1	1	−1	96.29
4	−1	1	1	49.64
5	0	0	−1.682	87.33
6	1	1	1	98.66
7	0	1.682	0	78.06
8	0	−1.682	0	76.93
9	1.682	0	0	99.90
10	0	0	0	90.83
11	0	0	0	90.83
12	1	−1	−1	96.40
13	−1	−1	−1	42.74
14	0	0	0	90.63
15	−1	−1	1	47.99
16	0	0	0	91.66
17	−1	1	−1	49.85
18	−1.682	0	0	16.28
19	0	0	0	90.94
20	1	−1	1	98.86

$$y = 90.97 + 24.94x_1 + 0.76x_2 + 0.93x_3 - 1.13x_1x_2 - 0.026x_1x_3 - 0.69x_2x_3$$
$$- 11.83x_1^2 - 4.97x_2^2 - 1.20x_3^2. \tag{4}$$

Statistical testing of this second-order model equation was carried out by analysis of variance (ANOVA); the results for removal rate are presented in Table 3. The model F-value of 1057.83 implies that the model was significant, being greater than $F_{0.01}(9, 10) = 4.94$, and the "Prob > F" value is less than 0.05. There was only a 0.01% chance that a model F-value this large could occur due to noise. The value of

Table 3 ANOVA for response surface quadratic model of removal rate

Source	Sum of squares	df	Mean square	F value	Prob $> F$
Model	10,758.99	9	1195.44	1057.83	<0.0001
Residual	11.30	10	1.13	–	–
Lack of fit	10.62	5	2.12	15.55	0.0046
Pure error	0.68	5	0.14	–	–

$R^2 = 0.9990$; Adj. $R^2 = 0.9980$

the coefficient of determination R^2 reached 0.9990, indicating that only 0.10% of the total variation was not expressed by this model. The value of the adjusted coefficient of determination reached 0.9980, also being close to 1 and indicating high significance of this model [33]. Significance testing for the coefficients of the equation with variables in terms of coded factors is presented in Table 4. "Prob $> F$" values below 0.05 indicate that the model terms were significant. In this case, Table 4 shows that the linear terms for CaO and MBFGA1, the CaO × MBFGA1 interaction term, and all the quadratic terms were significant for this model.

From the analysis above, it is obvious that the effect of the CaO × MBFGA1 interaction term was significant; thus, Fig. 4 shows the response surface plot for the effect of CaO and MBFGA1 on the removal rate (%), for stirring time of 60 min. According to the trend in this surface plot and the density of the bottom contour, as the dose of MBFGA1 was increased, the variation of the removal rate was very small at very low level of CaO; in contrast, at very high level of CaO, the removal rate showed almost no change as MBFGA1 was added, because the Ni(II) had basically been removed. Nevertheless, at the central level of CaO, the removal rate increased to a peak value then declined, indicating that this MBFGA1 dose was the most appropriate. In general, this phenomenon demonstrates that the CaO and MBFGA1 doses should be balanced for effective removal of Ni(II) from aqueous solution. In addition, when the CaO dose was at its central level, the MBFGA1 could effectively improve the removal rate of Ni(II), which could reach a higher level than the case with high CaO dose. Accordingly, the experimental results agree

Table 4 Significance of coefficients of quadratic model for removal rate

Variable	Coefficient estimate	df	Standard error	Prob $> F$
x_1	24.94	1	0.29	<0.0001
x_2	0.76	1	0.29	0.0250
x_3	0.93	1	0.29	0.0092
x_1x_2	−1.13	1	0.38	0.0130
x_1x_3	−0.026	1	0.38	0.9457
x_2x_3	−0.69	1	0.38	0.0947
x_1^2	−11.83	1	0.28	<0.0001
x_2^2	−4.97	1	0.28	<0.0001
x_3^2	−1.20	1	0.28	0.0016
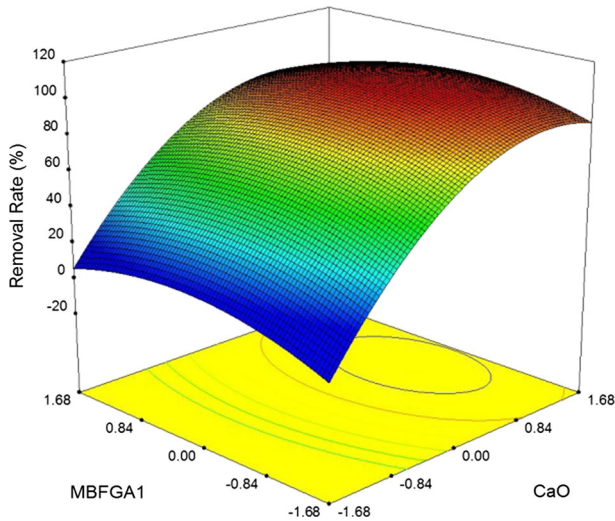
Fig. 4 Response surface plot for effect of CaO and MBFGA1 on removal rate (%)

with the analysis presented above: CaO at a central level corresponded to incomplete neutralization precipitation during the period of the zeta potential plateau; That is to say, for this condition, the collaboration between flocculation and biosorption was maximized.

According to the simultaneous targets of 100% removal rate and lowest CaO dose, to achieve the full flocculation and biosorption performance of MBFGA1 and enhance the Ni removal rate, the optimal conditions predicted from the regression equation were 1.3×10^{-2}% (w/w) CaO, 6.59×10^{-3}% (w/w) MBFGA1, and stirring time of 61.97 min, to achieve removal rate of 99.89% and biosorption capacity of 229.21 mg g^{-1}. For these conditions, the removal rate and biosorption capacity in verification tests reached 99.35% and 225.16 mg g^{-1}, respectively, and the concentration of Ni(II) was below 1 mg L^{-1} (national emission standard for pollutants for nickel industry, GB 25467-2010). Meanwhile, according to the calculation, the Ni(II) removal rate was increased by 15.10% by addition of MBFGA1. In addition, the biosorption capacity of MBFGA1 produced from *Paenibacillus polymyxa* GA1 was higher than for most other biomaterials reported in literature [34]. Hence, MBFGA1 may represent a significant biosorbent.

Biosorption behavior analysis

Analysis of biosorption isotherm during combined flocculation and biosorption

The Langmuir and Freundlich models [35, 36] were used in this study to simulate the biosorption process.

The Langmuir isotherm model is

$$q_e = K_L q_{max} C_e / (1 + K_L C_e). \tag{5}$$

The Freundlich isotherm model is

$$q_e = K_F C_e^{1/n}, \tag{6}$$

where C_e (mg L^{-1}) is the equilibrium concentration of Ni(II), and q_e (mg g^{-1}) is the amount of Ni(II) adsorbed, which can be calculated using Eq. (2). K_L (L g^{-1}) is the equilibrium adsorption constant. K_F and n are the Freundlich constants. q_{max} (mg g^{-1}) is the maximum amount of Ni(II) per unit mass of adsorbent.

Langmuir and Freundlich isotherm plots for Ni(II) biosorption are shown in Fig. 5, while the relevant parameters of the Langmuir and Freundlich isotherms are presented in Table 5. According to the correlation coefficient R^2 values, the Langmuir isotherm model provided better correlation compared with the Freundlich isotherm. Moreover, the maximum biosorption capacity calculated by the regression equation was close to the actual value; therefore, according to the Langmuir biosorption isotherm assumption, one can preliminary deduce that the biosorption behavior between MBFGA1 and Ni(II) exhibits a monolayer adsorption characteristic [30, 37].
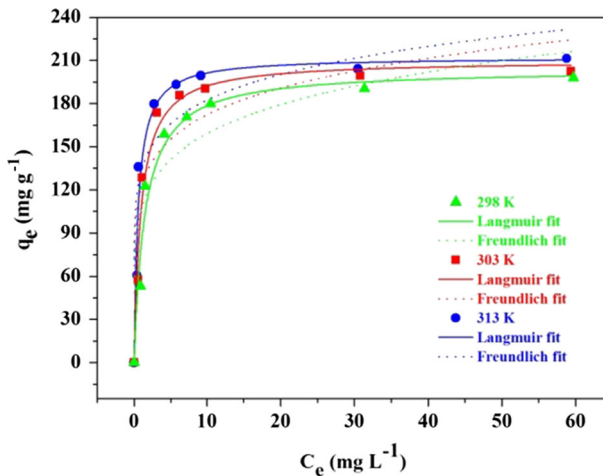
Fig. 5 Langmuir and Freundlich isotherm plots for Ni(II) biosorption

Table 5 Parameters of Langmuir and Freundlich biosorption isotherms

Temperature (K)	Langmuir isotherm model			Freundlich isotherm model		
	q_{max} (mg g^{-1})	K_L (L g^{-1})	R^2	K_F	n	R^2
298	204.05	0.6981	0.92	107.02	5.809	0.66
303	210.00	1.0868	0.93	122.43	6.745	0.61
313	212.27	1.8378	0.96	133.92	7.448	0.77

Analysis of biosorption kinetics during combined flocculation and biosorption

Pseudo-first-order and pseudo-second-order kinetic models [35, 38] were applied to simulate the biosorption process.

The equations can be expressed as follows:

$$q_t = q_e\left(1 - e^{-k_1 t}\right), \tag{7}$$

$$q_t = q_e^2 k_2 t / (1 + q_e k_2 t), \tag{8}$$

where k_1 (min^{-1}) and k_2 (g mg^{-1} min^{-1}) are the rate constant of the pseudo-first-order and pseudo-second-order kinetic model, and q_t and q_e are the amounts biosorbed (mg g^{-1}) at time t and equilibrium, respectively.

The fitting curves for these kinetic models are shown in Fig. 6. Table 6 shows that the correlation coefficient (R^2) of the pseudo-second-order kinetic model was higher than that of the pseudo-first-order kinetic model, indicating that the biosorption of Ni(II) onto MBFGA1 followed the pseudo-second-order kinetic model well. Furthermore, the values of q_e calculated from the pseudo-second-order kinetic model fit the experimental data better. Therefore, these experimental data suggest that biosorption of Ni(II) onto MBFGA1 mainly occurred via chemisorption or ion exchange [39].
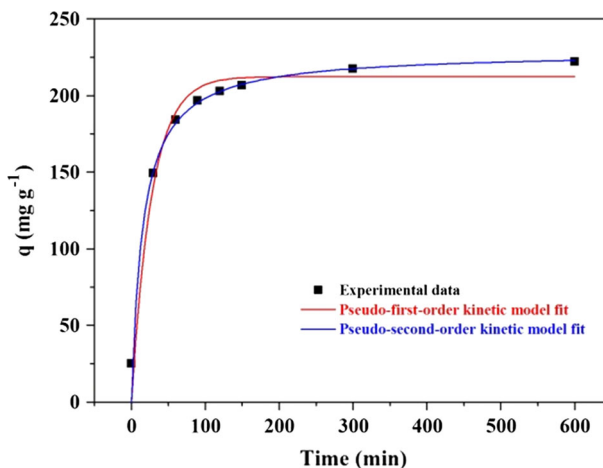
Fig. 6 Pseudo-first-order and pseudo-second-order kinetic models for Ni(II) biosorption

Table 6 Parameters of pseudo-first-order and pseudo-second-order kinetic models for Ni(II) biosorption

Temperature (K)	Pseudo-first-order			Pseudo-second-order		
	k_1 (min^{-1})	q_e (mg g^{-1})	R^2	k_2(g mg^{-1} min^{-1})	q_e (mg g^{-1})	R^2
313	0.03686	212.42	0.91	0.0002855	228.59	0.97

Analysis of biosorption thermodynamics during combined flocculation and biosorption

The thermodynamic parameters [30, 36, 37, 40] for the biosorption process were calculated by using the following equations:

$$\Delta G^\circ = -RT \ln K_D, \tag{9}$$

$$\Delta G^\circ = \Delta H^\circ - T\Delta S^\circ, \tag{10}$$

$$\ln K_D = \Delta S^\circ / R - \Delta H^\circ / RT, \tag{11}$$

where ΔG° (kJ mol^{-1}) is the Gibbs free energy change, ΔH° (kJ mol^{-1}) is the enthalpy change, ΔS° (J mol^{-1} K^{-1}) is the entropy change, R is the universal gas constant (8.314 J mol^{-1} K^{-1}), T (K) is the temperature, and K_D is the distribution coefficient, equal to q_e / C_e (L g^{-1}) [40]. The Gibbs free energy change of the process was related to the distribution coefficient (K_D) using the linearized form of Eq. (10). The values of ΔH° and ΔS° can then be determined from the intercept and slope of a linear plot of ΔG° versus T.

The calculated thermodynamic parameter values are presented in Table 7 and Fig. 7. The negative values of ΔG° at the three different temperatures suggest that the biosorption was spontaneous. In addition, the absolute values of ΔG° rose with increasing temperature (298, 303, and 313 K), indicating that high temperature could favor biosorption. Moreover, the positive values of ΔH° demonstrate that the biosorption process was endothermic. The positive values of ΔS° indicate increasing randomness at the solid–solution interface during biosorption.

Fourier-transform infrared (FT-IR) spectra analysis

The FT-IR spectra of the original and Ni(II)-loaded MBFGA1 in the range from 4000 to 400 cm^{-1} are compared in Fig. 8.

The spectrum of the original MBFGA1 shows many adsorption peaks, indicating the complex nature of the biomass examined. The adsorption peaks in the range

Table 7 Thermodynamic parameters for biosorption of Ni(II) onto MBFGA1

C_0 (mg/L)	ΔH° (kJ mol^{-1})	ΔS° (J mol^{-1} K^{-1})	ΔG° (kJ mol^{-1})			R^2
			298 K	303 K	313 K	
80	35.69	154.49	−10.16	−11.40	−12.57	0.92
85	39.19	168.16	−10.90	−11.79	−13.44	0.99
90	15.45	82.90	−9.06	−9.98	−10.40	0.70
95	8.46	55.13	−7.84	−8.42	−8.73	0.74
100	4.12	37.61	−7.04	−7.35	−7.63	0.90
120	0.02	15.17	−4.47	−4.63	−4.71	0.73
150	0.99	13.30	−2.97	−3.04	−3.17	0.99
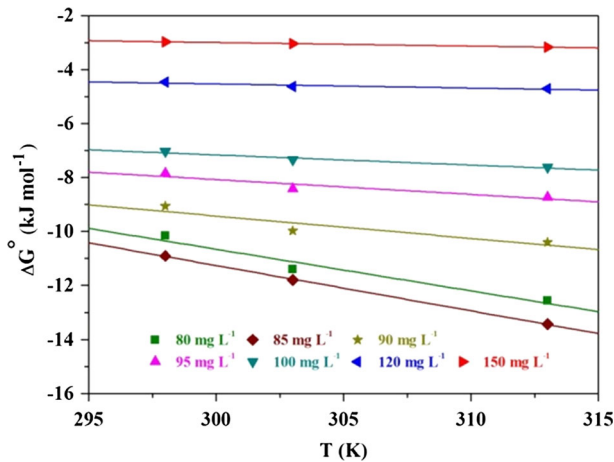
Fig. 7 Gibbs free energy change ($\Delta G°$) versus temperature (T)
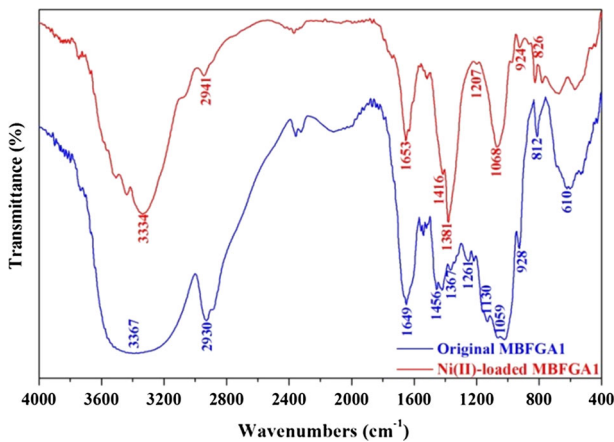
Fig. 8 Fourier-transform infrared spectra of original and Ni(II)-loaded MBFGA1

from 3600 to 3200 cm^{-1} correspond to stretching vibrations of O–H and N–H groups. Stretching vibrations of C–H, C=O, C–N, C–O–C, and C–O are indicated by the adsorption peaks at 2930, 1649, 1261, 1130, and 1059 cm^{-1}, respectively. Moreover, the adsorption peaks at 1456 and 1367 cm^{-1} correspond to asymmetric and symmetric bending of –CH$_2$– and –CH$_3$. The adsorption peaks at 928 and 812 cm^{-1} might correspond to stretching vibrations of glycosidic ring [27]. In summary, carboxyl, amine, and hydroxyl were the primary functional groups on MBFGA1, playing important roles in promoting biosorption of heavy-metal ions [41].

After Ni(II) biosorption, many adsorption peaks were obviously shifted with change in wavenumber and intensity, indicating binding of the functional groups

with Ni(II). The O–H and N–H stretching vibration shifted from 3367 cm^{-1} to 3334 cm^{-1}, indicating chemical interactions between Ni(II) and O–H and N–H groups on the surface of MBFGA1. Additionally, the peaks of C–H, C–N, and C–O groups shifted to 2941, 1207, and 1068 cm^{-1}, respectively. Moreover, the peaks corresponding to asymmetric and symmetric bending of –CH$_2$– and –CH$_3$ shifted to 1416 and 1381 cm^{-1}, respectively. Furthermore, the disappearance of the peak at 1130 cm^{-1} might be due to hydrolysis of glycosidic ring, in agreement with the increased intensity of O–H and C–O group signals. Moreover, the change of the peaks in the range from 800 to 400 cm^{-1} might be owing to ion exchange of carboxylic groups. In conclusion, the above-mentioned variations of the adsorption peaks suggest that hydroxyl, carboxyl, amino, acylamino, and polysaccharide played a key role in the Ni(II) adsorption onto MBFGA1.

Environmental scanning electron microscopy (ESEM) analysis

Figure 9a shows an ESEM image of flocs after adding alkaline reagent (CaO), and Fig. 9b after adding alkaline reagent (CaO) and MBFGA1, obtained in secondary-electron (SE) mode. Comparing these shows that the surface morphology of the flocs changed from smooth to coarse, while many granules could be seen on the
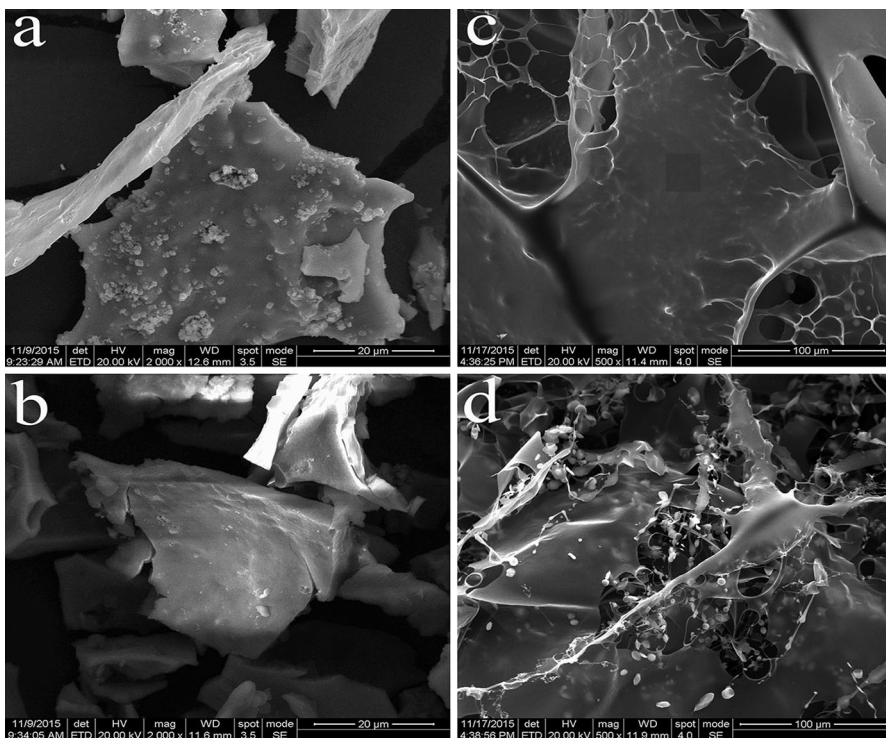
Fig. 9 ESEM images of: flocs after adding CaO at 2000× (**a**), CaO and MBFGA1 at 2000× (**b**), original MBFGA1 at 500× (**c**), and Ni(II)-loaded MBFGA1 at 500× (**d**)

surface of flocs after adding only CaO, possibly being Ca(OH)$_2$ or CaO. This analysis of the ESEM images and previous experimental data suggest that CaO plays a key role in the flocculation and biosorption by MBFGA1, which may provide more cores and adsorption sites. Figure 9c shows images of the original MBFGA1, which mainly showed smooth and flaky morphology with a small amount of filaments. In contrast, Fig. 9d shows images of Ni(II)-loaded MBFGA1, showing many filaments with tiny particles; one might speculate that this could be due to adsorption bridging of MBFGA1.

Results of EDS analysis in specific areas of the original and Ni(II)-loaded MBFGA1 are shown in Fig. 10. A small amount of phosphorus was detected in the
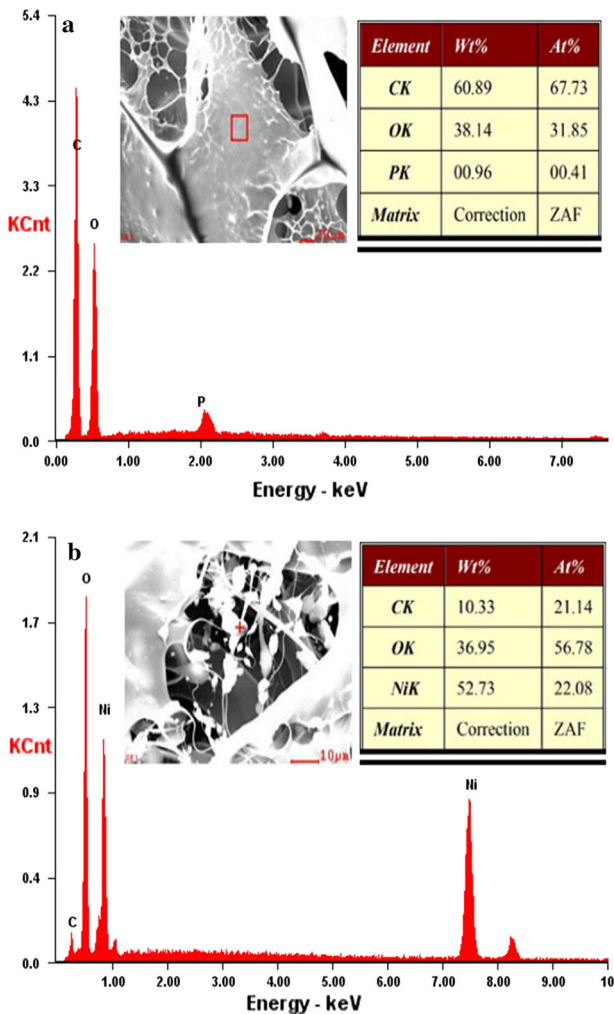
Fig. 10 Energy-dispersive spectrometry analysis of original MBFGA1 (**a**) and Ni(II)-loaded MBFGA1 (**b**)

area indicated in Fig. 10a, possibly coming from the fermentation liquid. As shown in Fig. 10b, the Ni(II) content reached 52.73% in the detection area of filaments with tiny particles. These results suggest that such filaments play an important role in the biosorption and may take up Ni(II). Furthermore, these analyses clearly prove that Ni(II) was bound onto the MBFGA1 with strong linkage; simultaneously, one can assume that adsorption bridging might be the main biosorption mechanism exhibited by MBFGA1.

Mechanism and procedure of collaboration between flocculation and biosorption

Figure 11 shows a mechanism and procedure proposed for the collaboration between flocculation and biosorption. Firstly, the clustered molecular chain structure of MBFGA1 stretched to form a linear structure because of sufficient OH^- in aqueous solution, which would benefit flocculation and biosorption. Secondly, when ion exchange occurred, Ni(II) and Ca^{2+} were absorbed onto
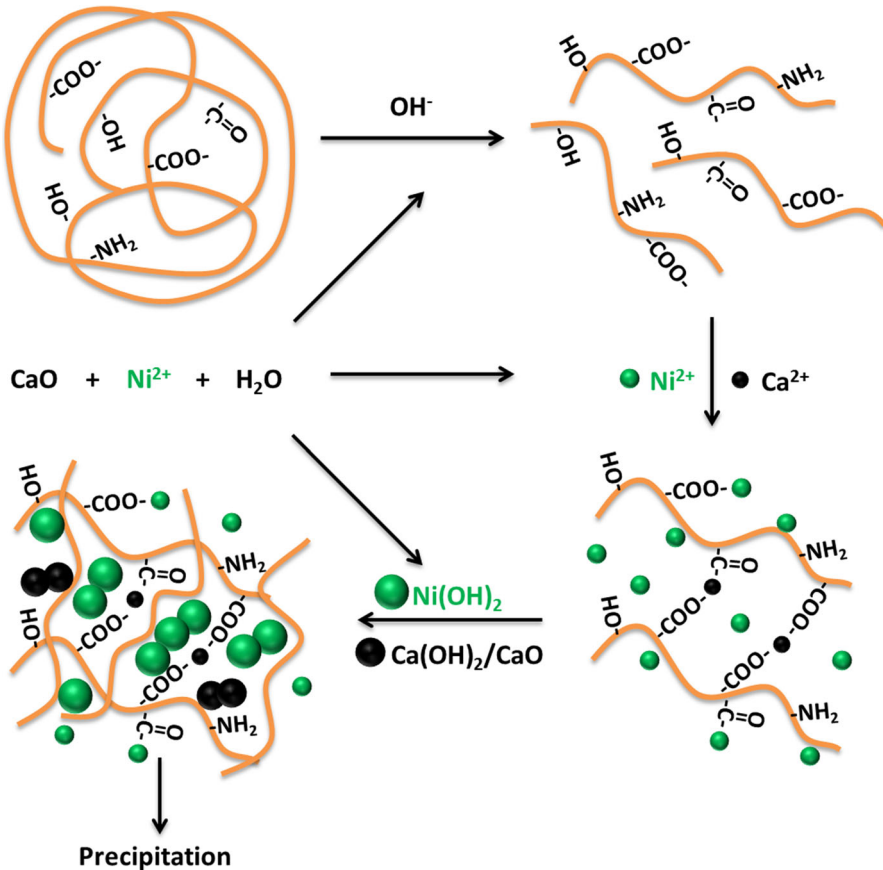
Fig. 11 Mechanism and procedure of collaboration between flocculation and biosorption

MBFGA1 by polar groups such as carboxyl and methoxyl, while at the same time, Ca^{2+} could reduce the distance between particles, facilitating absorption of Ni(II) ions by MBFGA1. Thirdly, the generated metal hydroxides and some undissolved CaO aggregated, potentially acting as cores of flocs. Furthermore, after absorbing Ni(II) ions, MBFGA1 might adhere to the surface of flocs and its different molecular chains would connect together, resulting in formation of larger floc particles from the aggregates and ultimately coprecipitation. This figure and the analyses presented above indicate that adsorption bridging with precipitation enmeshment was the main mechanism; flocculation and biosorption by MBFGA1 therefore supplemented each other and had a close relationship, with their collaboration having a significant effect on the Ni(II) removal process.

Conclusions

The collaboration between flocculation and biosorption by MBFGA1 was fully utilized to achieve improved Ni(II) removal. When alkaline reagents were added to Ni(II)-containing wastewater, the period of zeta potential plateau was an appropriate time at which the full biosorption performance of MBFGA1 could be used and the pH was relatively low. CaO was found to be a better alkaline reagent compared with NaOH, playing an important role in promoting flocculation and biosorption by MBFGA1.

According to the response surface methodology results, the optimal conditions for flocculation and biosorption calculated from the regression equation were 1.3×10^{-2}% (w/w) CaO, 6.59×10^{-3}% (w/w) MBFGA1, and stirring time of 61.97 min, at which the Ni(II) removal rate and biosorption capacity of MBFGA1 could reach 99.35% and 225.16 mg g^{-1}, respectively.

For biosorption by MBFGA1, the Langmuir adsorption isotherm model presented better correlation compared with the Freundlich adsorption isotherm model, and the pseudo-second-order kinetic model fit the experimental data better than the pseudo-first-order kinetic model. Furthermore, FT-IR and ESEM analyses suggested that hydroxyl, carboxyl, amino, acylamino, and polysaccharide played key roles in Ni(II) biosorption onto MBFGA1. Analysis of the mechanism and procedure indicated that adsorption bridging with precipitation enmeshment was vital during the flocculation and biosorption process.

References

1. U.K. Garg, M. Kaur, V. Garg, D. Sud, Bioresour. Technol. **99**, 1325–1331 (2008)
2. A. Bhatnagar, A. Minocha, Colloids Surf. B **76**, 544–548 (2010)
3. E. Denkhaus, K. Salnikov, Crit. Rev. Oncol. Hematol. **42**, 35–56 (2002)
4. N. Boujelben, J. Bouzid, Z. Elouear, J. Hazard. Mater. **163**, 376–382 (2009)
5. K.S. Kasprzak, F.W. Sunderman, K. Salnikow, Mutat. Res-Fund. Mol. M. **533**, 67–97 (2003)
6. M. Jiang, X. Jin, X. Lu, Z. Chen, Desalination **252**, 33–39 (2010)

7. C. Quintelas, Z. Rocha, B. Silva, B. Fonseca, H. Figueiredo, T. Tavares, Chem. Eng. J. **152**, 110–115 (2009)
8. E. Malkoc, Y. Nuhoglu, J. Hazard. Mater. **127**, 120–128 (2005)
9. M.I. Kandah, J.L. Meunier, J. Hazard. Mater. **146**, 283–288 (2007)
10. M. Zhao, Y. Xu, C. Zhang, H. Rong, G. Zeng, Appl. Microbiol. Biotechnol. **100**, 6509–6518 (2016)
11. A. Papadopoulos, D. Fatta, K. Parperis, A. Mentzis, K.J. Haralambous, M. Loizidou, Sep. Purif. Technol. **39**, 181–188 (2004)
12. I. Kabdaşlı, T. Arslan, T. Ölmez-Hancı, I. Arslan-Alaton, O. Tünay, J. Hazard. Mater. **165**, 838–845 (2009)
13. K. Dermentzis, J. Hazard. Mater. **173**, 647–652 (2009)
14. M. Belkacem, M. Khodir, S. Abdelkrim, Desalination **228**, 245–254 (2008)
15. V. Coman, B. Robotin, P. Ilea, Resour. Conserv. Recycl. **73**, 229–238 (2013)
16. H. Salehizadeh, S. Shojaosadati, Biotechnol. Adv. **19**, 371–385 (2001)
17. Z. Yang, J. Huang, G. Zeng, M. Ruan, C. Zhou, L. Li, Z. Rong, Bioresour. Technol. **100**, 4233–4239 (2009)
18. C. Exley, O. Korchazhkina, D. Job, S. Strekopytov, A. Polwart, P. Crome, J. Alzheimer's Dis. **10**, 17–24 (2006)
19. C. Rudén, Food Chem. Toxicol. **42**, 335–349 (2004)
20. K.L. Dearfield, C.O. Abernathy, M.S. Ottley, J.H. Brantner, P.F. Hayes, Mutat. Res. Genet. Toxicol. **195**, 45–77 (1988)
21. M.D. Machado, M.S. Santos, C. Gouveia, H.M. Soares, E.V. Soares, Bioresour. Technol. **99**, 2107–2115 (2008)
22. A.M. Azzam, A. Tawfik, J. Environ. Eng. Landsc. Manag. **23**, 288–294 (2015)
23. E.Z. Gomaa, Pol. J. Microbiol. **61**, 281–289 (2012)
24. F. Fu, Q. Wang, J. Environ. Manag. **92**, 407–418 (2011)
25. L. Charerntanyarak, Water Sci. Technol. **39**, 135–138 (1999)
26. A. El Samrani, B. Lartiges, F. Villiéras, Water Res. **42**, 951–960 (2008)
27. J. Huang, Z. Yang, G. Zeng, M. Ruan, H. Xu, W. Gao, Y. Luo, H. Xie, Chem. Eng. J. **191**, 269–277 (2012)
28. Z. Yang, Z. Wu, G. Zeng, J. Huang, H. Xu, J. Feng, P. Song, M. Li, L. Wang, RSC Adv. **4**, 40464–40473 (2014)
29. I. Shih, Y. Van, L. Yeh, H. Lin, Y. Chang, Bioresour. Technol. **78**, 267–272 (2001)
30. J. Feng, Z. Yang, G. Zeng, J. Huang, H. Xu, Y. Zhang, S. Wei, L. Wang, Bioresour. Technol. **148**, 414–421 (2013)
31. W. Liu, H. Yuan, J. Yang, B. Li, Bioresour. Technol. **100**, 2629–2632 (2009)
32. Z. Li, S. Zhong, H. Lei, R. Chen, Q. Yu, H. Li, Bioresour. Technol. **100**, 3650–3656 (2009)
33. M. Elibol, Process Biochem. **38**, 667–673 (2002)
34. A. Thevannan, R. Mungroo, C.H. Niu, Bioresour. Technol. **101**, 1776–1780 (2010)
35. M. Torab-Mostaedi, M. Asadollahzadeh, A. Hemmati, A. Khosravi, J. Taiwan Inst. Chem. Eng. **44**, 295–302 (2013)
36. A. Olgun, N. Atar, J. Ind. Eng. Chem. **18**, 1751–1757 (2012)
37. J. Hu, J. Wang, Y. Liu, X. Li, G. Zeng, Z. Bao, X. Zeng, A. Chen, X. Long, J. Hazard. Mater. **185**, 306–314 (2011)
38. M. Moyo, S.T. Lindiwe, E. Sebata, B.C. Nyamunda, U. Guyo, Res. Chem. Intermed. **42**, 1349–1362 (2016)
39. Y.A. Aydın, N.D. Aksoy, Chem. Eng. J. **151**, 188–194 (2009)
40. A. Sarı, M. Tuzen, Ö.D. Uluözlü, M. Soylak, Biochem. Eng. J. **37**, 151–158 (2007)
41. D. Park, Y.-S. Yun, J.M. Park, Biotechnol. Bioprocess Eng. **15**, 86–102 (2010)